Solvation pressure as real pressure: I. Ethanol and starch under negative pressure

2003 J. Phys.: Condens. Matter 15 1577

(http://iopscience.iop.org/0953-8984/15/10/306)

INSTITUTE OF PHYSICS PUBLISHING JOURNAL OF PHYSICS: CONDENSED MATTER

J. Phys.: Condens. Matter **15** (2003) 1577–1584 PII: S0953-8984(03)40026-X

Solvation pressure as real pressure: I. Ethanol and starch under negative pressure

N W A van Uden[1], H Hubel[1], D A Faux[2], A C Tanczos[3], B Howlin[3] and D J Dunstan[1]

[1] Physics Department, Queen Mary, University of London, London E1 4NS, UK
[2] Physics Department, University of Surrey, Guildford GU2 7XH, UK
[3] Chemistry Department, University of Surrey, Guildford GU2 7XH, UK

Received 30 July 2002, in final form 30 January 2003
Published 3 March 2003
Online at stacks.iop.org/JPhysCM/15/1577

Abstract

The reality of the solvation pressure generated by the cohesive energy density of liquids is demonstrated by three methods. Firstly, the Raman spectrum of ethanol as a function of cohesive energy density (solvation pressure) in ethanol–water and ethanol–chloroform mixtures is compared with the Raman spectrum of pure ethanol under external hydrostatic pressure and the solvation pressure and hydrostatic pressure are found to be equivalent for some transitions. Secondly, the bond lengths of ethanol are calculated by molecular dynamics modelling for liquid ethanol under pressure and for ethanol vapour. The difference in bond lengths between vapour and liquid are found to be equivalent to the solvation pressure for the C–H_3, C–H_2 and O–H bond lengths, with discrepancies for the C–C and C–O bond lengths. Thirdly, the pressure-induced gelation of potato starch is measured in pure water and in mixtures of water and ethanol. The phase transition pressure varies in accordance with the change in solvation pressure of the solvent. These results demonstrate the reality of 'negative pressures' generated by reductions in the cohesive energy density of solvent mixtures.

1. Introduction

In previous papers we reported that the cohesive energy density of a liquid acts on nanoparticles in the same way as hydrostatic pressure, indicating that the cohesive energy density is in some way equivalent to a real pressure, which we call here solvation pressure (Wood *et al* 1999, 2000). Dixit *et al* (2000) suggested that the effect could be observed on molecules in liquid mixtures. In this paper we follow their suggestion, studying the solvation pressure on ethanol molecules in the presence of co-solvents by Raman spectroscopy. We report molecular dynamics (MD) modelling of ethanol liquid and vapour, which confirms the solvation pressure of the pure liquid. Finally, in accordance with these results, the admixture of ethanol is observed to increase the

gelation pressure of starch grains in aqueous solution. Within our interpretation, this constitutes the first observation of a biological molecule under negative hydrostatic pressure.

The cohesive energy density (CED) of a liquid is a quantity derived from the energy of evaporation per unit volume, and ranges from a few hundred MPa for non-polar solvents up to 2294 MPa for water (Grulke 1998). The CED of a mixture of two liquids is estimated here as a linear interpolation with volume fraction of the two components in the mixture:

$$\mathrm{CED}_{\mathrm{mixture}} = \frac{V_1\mathrm{CED}_1 + V_2\mathrm{CED}_2}{V_1 + V_2}. \tag{1}$$

The difference between the CED of the mixture and the CED of one of the components is the solvation pressure applied to that component:

$$\begin{aligned} P_1 &= \frac{V_2}{V_1 + V_2}(\mathrm{CED}_2 - \mathrm{CED}_1) \\ P_2 &= \frac{V_1}{V_1 + V_2}(\mathrm{CED}_1 - \mathrm{CED}_2). \end{aligned} \tag{2}$$

Hence, if the CED of the other component is smaller than the CED of the component of interest, one is actually able to apply a negative solvation pressure.

In this paper we use Raman spectroscopy to monitor the effect of solvation and hydrostatic pressure on the Raman frequencies of ethanol. The solvation pressures are obtained by mixing ethanol (CED = 676 MPa) with both a higher- and a lower-CED liquid, namely water (CED = 2294 MPa) and chloroform (CED = 361 MPa). Hydrostatic pressure is also applied to ethanol. We use MD simulations to calculate bond lengths and we use the gelation transition pressure of starch to reveal changes in the solvation pressure of water–ethanol mixtures.

2. Experimental techniques

2.1. Sample preparation

GPR grade ethanol from Merck and Analar grade chloroform from Romil were used as purchased. Ethanol was mixed with distilled water and chloroform by volume at room temperature. The mixtures were kept in sealed sample containers and used within 12 h.

Potato starch grains, which have previously been studied by Rubens *et al* (1999), were dispersed in distilled water and in water–ethanol mixtures. Under pressure, their gelation was detected by optical microscopy.

2.2. Raman spectroscopy

Raman spectra of liquid ethanol and the various mixtures were recorded using a Renishaw Raman microscope system. The excitation source was a 60 mW He–Ne laser with a wavelength of 632.8 nm. The Raman signal was collected in the backscattering geometry. The spectral range was 300–3500 cm^{-1} shift. The spectral resolution was better than 1 cm^{-1}. The Raman frequencies were standardized using the emission lines of a neon lamp.

2.3. High-pressure measurements

High pressure was generated using a miniature diamond-anvil cell (DAC) (Dunstan and Scherrer 1988) modified to operate with only one anvil giving access to a relatively low-pressure range easily controllable from atmospheric pressure up to 1.5 GPa (van Uden and Dunstan 2000). Pressure was determined from the photoluminescence (PL) of ruby. With a

Table 1. Labels of the Raman modes are listed together with the description of the corresponding modes, their Raman frequencies, hydrostatic pressure dependences and offset values used in figure 1.

Label	Raman modes	Peak position (cm^{-1})	Pressure dependence (cm^{-1} $kbar^{-1}$)	Vertical offset (cm^{-1})
CH_3s	CH_3 stretch	2928.7	1.13	0
CH_2	CH_2 symmetric stretch	2880.6	0.99	3
CH_3d	CH_3 deformation	1453.7	0.26	6
MO_1	CH_2 twist + in plane COH deformation	1275.7	0.37	9
MO_2	CO stretch +CH_3 rock + in plane COH deformation	1095.5	−0.58	12
CCOa	CCO anti symmetric stretch	1050.8	0.50	15
CCOs	CCO symmetric stretch	883.1	0.51	18

632.8 nm He–Ne laser Raman system, the ruby PL at 694 nm is conveniently at 1400 cm^{-1}. A small ruby chip was placed inside the high-pressure cell and its PL spectrum was recorded and compared with the PL spectrum of an external reference piece of ruby at atmospheric pressure. The shift between the PL peaks of the cell and reference ruby were used to calculate the pressure inside the sample volume. The peak position of the ruby could be determined with an accuracy of 0.3 cm^{-1}, which corresponds to 0.04 GPa.

A dilute suspension of starch grains was used so that a few grains could be visually identified in the DAC. The starch grains were not easily seen in the single-anvil cell with illumination from above. For these experiments, a thick gasket was used in a DAC so that illumination from below could be used. The gelation was then clearly visible.

3. Experimental results

The ethanol Raman peak positions are plotted as a function of the total pressure, solvation plus external pressure, and are shown in figure 1. In figure 1(a), the mode labelled CH_3s (see table 1) responds to the solvation pressure of water (△) at the same rate as the shifts with hydrostatic pressure. The same is true for the modes labelled CH_2, CH_3d, MO_1 and MO_2 (see table 1). The ◊ data points show that the MO_1, CCOa and CCOs have a similar behaviour with the chloroform solvation presssure.

However in figure 1(b) we see that not all data behaves in this way. Apart from MO_1, each of the other modes behave either with chloroform or water quite differently from their hydrostatic pressure shifts. Note that water–CCO modes and chloroform–CH_x modes predominate in figure 1(b), while modes of the hydrophobic part of ethanol in water and modes of the hydrophilic part of ethanol in chloroform dominate figure 1(a). We return to this point in section 5.

Results for the starch gelation are shown in figure 2. Rubens *et al* (1999) reported the transition at 0.65 GPa in pure water. Plotting the solvation pressures of the ethanol–water mixtures against the external pressures at which gelation occurs yields within scatter a straight line with a slope close to −1. This indicates that the gelation transition occurs at a constant value of $P_{ext} + P_{sol} = P_t$, and therefore that the solvation pressure and the external pressure act upon starch in the same way.

4. Molecular dynamics modelling

MD simulations were carried out on 100 ethanol molecules at 298 K contained in a simulation cube with sides of about 2 nm. Periodic boundary conditions were used throughout. The

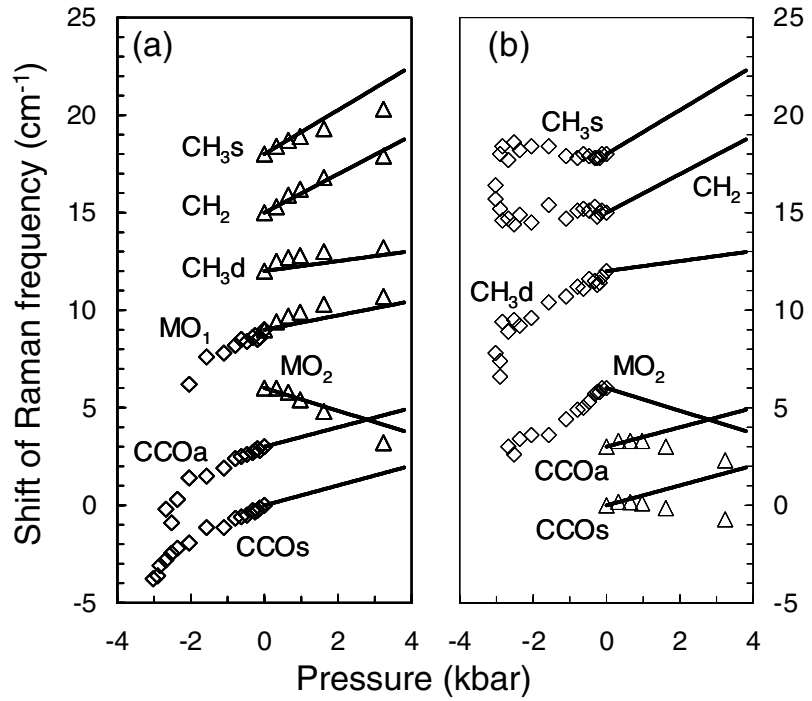

Figure 1. The shifts in ethanol Raman peak frequencies are plotted against the solvation pressure of various liquid mixtures, water–ethanol (△) and chloroform–ethanol (◇). The Raman mode frequencies and labels are given in table 1. The data are offset vertically for clarity. The solid lines represent the linear term in the hydrostatic pressure dependence (table 1) of the Raman peaks. In (a) those data for which solvation pressure acts as hydrostatic pressure are shown, while data showing more complicated behaviour are shown in (b).

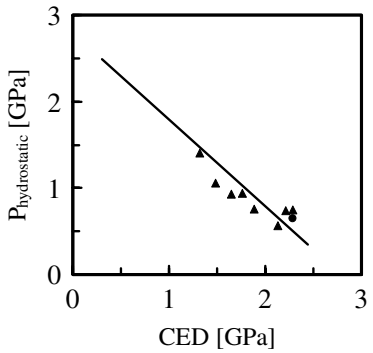

Figure 2. The data points indicate the gelation of the starch granules in various ethanol–water mixtures. The solvation pressures of the mixtures are plotted against the external pressures at which gelation occurs. The straight line is a guide to the eye with the slope −1 expected if solvation pressure acts exactly as real pressure. The solid circle is taken from Rubens *et al* (1999).

intramolecular potentials consisted of Morse two-body, harmonic three-body and dihedral four-body terms and the intermolecular potentials comprised Lennard-Jones (12–6) and Coulombic

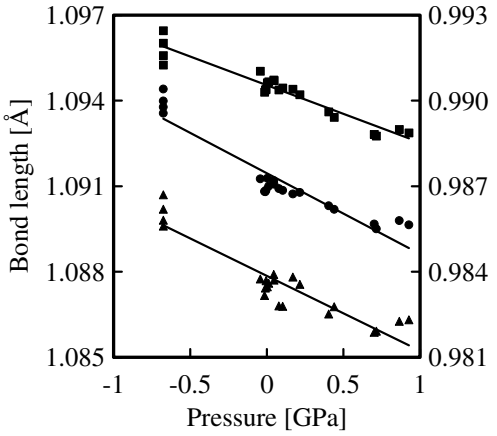

Figure 3. Bond lengths calculated from MD are plotted against pressure. The vapour phase values are plotted at −676 MPa, corresponding to the solvation pressure. The straight lines are guides to the eye. For the C–H_3 (■ on the left-hand axis), C–H_2 (● on the left-hand axis and with an offset of −0.003 Å) and O–H (▲ on the right-hand axis) bonds, the vapour phase data fall close to the straight lines.

two-body terms, plus a Lennard-Jones (12–10) term to approximate the hydrogen bonding. All parameters are given by the DREIDING potential set (Mayo *et al* 1990). Point effective Gasteiger charges (Gasteiger and Marsili 1980) are assigned and are, in units of e, 0.025 (H on C–H_3), 0.057 (H on C–H_2), −0.042 (C on C–H_3), 0.040 (C on C–H_2), −0.397 (O) and 0.21 (H on O–H). The Ewald summation technique was used to determine the long-range Coulomb interactions and the non-Coulombic intermolecular potentials were cut off at 0.95 nm.

The MD simulations were performed using DLPOLY version 2.13 (Smith and Forester 1996). Configurations were obtained corresponding to different pressures by executing NPT ensemble simulations with a target pressure of 3 GPa for 20 000 time steps using a small time interval of 0.0002 fs. The Berendsen barostat was used with thermostat and barostat relaxation times of 0.1 ps. To ensure equilibrium at each new volume, MD simulations were performed using thermostated Nosé–Hoover NVT dynamics using velocity rescaling for equilibration to a total time in excess of 10 ps. The sequence of NPT–NVT simulations was repeated to obtain equilibrium configurations over the range −0.05–1.8 GPa. For the vapour phase, simulations were performed on a single molecule.

The density of the liquid at ambient pressure was calculated to be 0.85 g cm^{-3}, about 8% higher than the true value of 0.785 g cm^{-3}. The compressibility was 1.15 ± 0.17 GPa^{-1} in good agreement within error with the established value of 1.12 GPa^{-1}.

The main simulations comprised 10^5 time steps of 0.2 fs at each pressure. Velocity data were output every 25 time steps enabling vibrational spectra to be obtained over the range 0–3300 cm^{-1} at a resolution of 3.33 cm^{-1}.

Vibrational spectra were obtained as the Fourier transforms of the velocity autocorrelation functions averaged over all atoms. Averaging over single atoms could be used to help identify the peaks in the spectra. Preliminary results are in agreement with Perchard and Josien (1968), Dollish *et al* (1974) and Tewell *et al* (2002). Absolute frequencies are accurate to within, typically, 100 cm^{-1}, so we have confidence in the bondlengths presented here. Pressure and solvent effects on the frequencies are not yet available and will be presented elsewhere.

In figure 3, the mean bond lengths of the C–H_3, C–H_2 and O–H bonds are shown, plotted against pressure. The vapour phase data are plotted at −676 MPa, in accordance with the

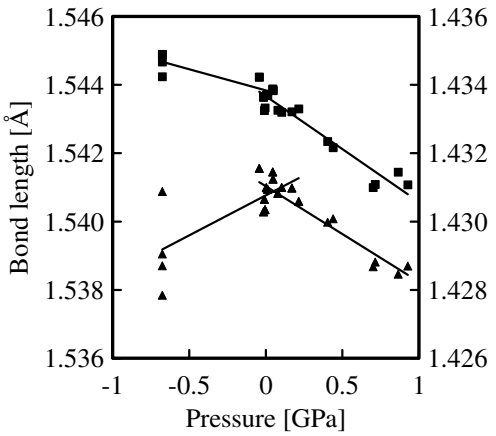

Figure 4. Bond lengths calculated from MD are plotted against pressure. The vapour phase values are plotted at −676 Mpa, corresponding to the solvation pressure. The straight lines are guides to the eye. For the C–O (▲ on the right-hand axis) and C–C (■ on the left-hand axis) bonds, the vapour phase data deviate significantly from the pressure data.

attribution of the full solvation pressure to the liquid at ambient pressure. The mean bond lengths in the vapour fall on a straight-line fit through the liquid pressure data, demonstrating that the change in the bond lengths is consistent with the interpretation of the solvation pressure as equivalent to a hydrostatic pressure of −676 MPa. This is not the case for all of the bonds. The data for the C–C and C–O bond lengths, plotted in figure 4, fit less well to straight lines through the liquid pressure data. Noticeably, the C–O bond length is significantly *longer* in the liquid compared to the vapour.

5. Discussion

It remains to understand, first, how solvation pressure can exert a real pressure on solutes, and second, why the effect is seen only upon some Raman peaks and bond lengths and not on others. What follows on these two points is highly speculative.

Cohesive energy density is E/V, where E is the molar energy of evaporation and V is the molar volume. The internal pressure of a liquid is a useful thermodynamic parameter defined as $\partial E/\partial V$, and Hildebrand and Scott (1950) devotes some attention to the question when these two quantities may be the same. It may be that our solvation pressure should be equated with the internal pressure rather than the cohesive energy density. We can find no suggestion in the literature, however, that the internal pressure may itself act as a real pressure. If we regard a liquid as a highly condensed gas, there may be a clue in the van der Waals gas equation with its pressure term due to attractive intermolecular forces. The literature on this is very confusing and arguments why the walls of the container should see the pressure $(P - aV^{-2})$ while the gas (or liquid) molecules should see the pressure P are inconclusive. Indeed, Tabor (1991) states that the van der Waals equation 'holds better than it ought'.

Hutchinson and Ben-Amotz (1998) and Meléndez-Pagán and Ben-Amotz (2000) predict that bond lengths should be shorter in liquid than in vapour, on the general argument that the attractive forces are long-range while the repulsive forces are short-range. To illustrate this argument we write the attractive intermolecular potential as

$$u(r) \propto -r^{-x}. \tag{3}$$

The cohesive energy density (solvation pressure) is then calculated as $u(r)$ divided by the volume of the molecule, a sphere of radius $\frac{1}{2}r$

$$\mathrm{CED} = \frac{-r^{-x}}{\frac{4}{24}\pi r^3}. \tag{4}$$

The pressure is calculated by dividing the derivative $u'(r)$ by the surface area of the same sphere

$$P = -\frac{xr^{-x-1}}{\pi r^2}. \tag{5}$$

Equating the cohesive energy density with pressure and solving for x gives $x = 6$. The identity of the solvation pressure with real pressure may therefore be due simply to the Lennard-Jones 12–6 potential and its good fit to reality, where we note that the r^{-6} long-range attractive term is derived from quantum mechanics. Further theoretical exploration is required.

These arguments all suggest that, if real, solvation pressure is due to inter-molecular potentials. It would be expected to act equally upon all intra-molecular bonds and vibrational frequencies in the solute. However, there are additional interactions between solvent and solute molecules which perturb the intra-molecular potentials in the solute—in the limit, the formation of new chemical bonds between solvent and solute, with consequent rearrangement of the solute intra-molecular bonding. Hydrogen bonding in our water–ethanol mixtures is a good example of this. Hydrogen bonding in the water would contribute, of course, to the solvation pressure on the ethanol molecules; thereby putting the whole ethanol molecule under pressure and reducing all bond lengths. In addition, hydrogen bonding between H_2O and C_2H_5OH molecules increases the ethanol OH bond length, with consequent perturbations to the CO bond and weaker effects further along the ethanol molecule. This will cause large shifts in the bond lengths and the corresponding Raman frequencies, as seen in figure 1(b), and completely masking any solvation pressure effect. The CH_x bonds are least perturbed and so the Raman peaks corresponding to these bond stretches is expected to provide the most accurate solvation pressure barometer, as seen in figure 1(a). Different interactions between the ethanol and chloroform would be expected to cause different Raman frequencies and bond-lengths to deviate from the simple dependence solvation pressure, so that CO and OH bonds will participate in the vibrations, which are the best solvation pressure barometer in chloroform (figure 1(a)).

6. Conclusion

These results constitute three strong and independent items of evidence that the cohesive energy density is a real pressure, a solvation pressure. In ethanol, the experimental Raman shifts, and the MD vibrational frequencies and bond lengths, in some cases, vary with solvation pressure in the same way as they do with real pressure. The gelation of starch occurs at constant value of real pressure plus solvation pressure, and so the addition of ethanol as a co-solvent represents the application of a negative hydrostatic pressure to this biological molecule. Further molecular dynamics modelling of the liquid mixtures is required to understand these phenomena fully.

Acknowledgments

The authors are grateful to Queen Mary, University of London, and EPSRC for funding. Special thanks go to Dr M D Frogley, Dr J R Wood and Professor W C K Poon for stimulating this work. For assistance with the starch gelation experiment we would like to thank Dr F Meersman and Professor K Heremans.

References

Dixit S, Poon W C K and Crain J 2000 *J. Phys.: Condens. Matter* **12** L323–8
Dollish F R, Fateley W G and Bentley F F 1974 *Characteristic Raman Frequencies of Organic Compounds* (New York: Wiley) pp 27–34
Dunstan D J and Scherrer W 1988 *Rev. Sci. Instrum.* **59** 627–30
Dunstan D J, van Uden N W A and Ackland G J 2002 *High Pressure Res.* **22** 773–8
Gasteiger J and Marsili M 1980 *Tetrahedron* **36** 3219–27
Grulke E A 1998 *Polymer Handbook* 4th edn, ed J Brandrup and E H Immergut (New York: Wiley) pp 675–714
Hildebrand J H and Scott R L 1950 *The Solubility of Nonelectrolytes* 3rd edn (Princeton, NJ: Reinhold) pp 97–9
Hutchinson E J and Ben-Amotz D 1998 *J. Phys. Chem.* B **102** 3354–62
Mayo S L, Olafson B D and Goddard W A 1990 *J. Phys. Chem.* **94** 8897–909
Meléndez-Pagán Y and Ben-Amotz D 2000 *J. Phys. Chem.* B **104** 7858–66
Perchard J P and Josien M L 1968 *J. Chim. Phys.* **65** 1834–55
Perchard J P and Josien M L 1968 *J. Chim. Phys.* **65** 1856–75
Rubens P, Snauwaert J, Heremans K and Stute R 1999 *Carbohydr. Polym.* **39** 231–5
Smith W and Forester T R 1996 *J. Mol. Graphics* **14** 136
Tabor D 1991 *Gases, Liquids and Solids and Other States of Matter* 3rd edn (Cambridge: Cambridge University Press) p 130
Tewell C R, Malizia F, Ager J W III and Somorjai G A 2002 *J. Phys. Chem.* B **106** 2946–9
van Uden N W A and Dunstan D J 2000 *Rev. Sci. Instrum.* **71** 4174–6
Wood J R, Frogley M D, Meurs E R, Prins A D, Peijs T, Dunstan D J and Wagner H D 1999 *J. Phys. Chem.* B **103** 10388–92
Wood J R, Frogley M D, Meurs E R, Prins A D, Peijs T, Dunstan D J and Wagner H D 2000 *High Pressure Res.* **18** 153
Wood J R, Zhao Q, Frogley M D, Meurs E R, Prins A D, Peijs T, Dunstan D J and Wagner H D 2000 *Phys. Rev.* B **62** 7571–5